Hindawi
Geofluids
Volume 2020, Article ID 2359740, 14 pages
https://doi.org/10.1155/2020/2359740

Research Article

Mantle-Derived Helium Emission near the Pohang EGS Site, South Korea: Implications for Active Fault Distribution

Heejun Kim,[1] Hyunwoo Lee,[1] Jaemin Lee,[2,3] Hyun A. Lee,[2] Nam Chil Woo,[2] Youn-Soo Lee,[4] Takanori Kagoshima,[5] Naoto Takahata,[5] and Yuji Sano[5,6]

[1]*School of Earth and Environmental Sciences, Seoul National University, Seoul 08826, Republic of Korea*
[2]*Department of Earth System Sciences, Yonsei University, Seoul 03722, Republic of Korea*
[3]*Korea Institute of Geoscience and Mineral Resources, Daejeon 34132, Republic of Korea*
[4]*Division of Environmental Science and Engineering, Pohang University of Science and Technology, Pohang 37673, Republic of Korea*
[5]*Atmosphere and Ocean Research Institute, University of Tokyo, Kashiwa, Chiba 277-8564, Japan*
[6]*Institute of Surface-Earth System Science, Tianjin University, Tianjin 300072, China*

Correspondence should be addressed to Hyunwoo Lee; lhw615@snu.ac.kr

Received 18 February 2020; Revised 3 July 2020; Accepted 6 July 2020; Published 24 July 2020

Academic Editor: Ondra Sracek

An Mw 5.5 earthquake occurred in Pohang, South Korea on November 15, 2017, resulting in a great impact on society. Despite a lot of controversy about the cause of the earthquake in relation to the enhanced geothermal system (EGS), the location of earthquake-related active faults is poorly known. Here, we first report the results of the geochemical and isotopic analyses of dissolved gases in groundwater in the Heunghae, Yeonil, and Sinkwang areas. According to the N_2-Ar-He relationship, samples from the Heunghae and Yeonil areas are contributed to the mantle, except for the Sinkwang area, where all samples are atmospheric. The Pohang samples consist mainly of N_2 and CO_2, and some samples of the Heunghae and Yeonil areas contain substantial CH_4. Stable isotope compositions of N_2 ($\delta^{15}N = 0.2$ to 3.6‰), CO_2 ($\delta^{13}C = -27.3$ to -16.0‰), and CH_4 ($\delta^{13}C = -76.1$ to -70.0‰) indicate that these components are derived from organic substances in sedimentary layer of Pohang Basin. On the other hand, helium isotope ratios ($^3He/^4He$, up to 3.83 Ra) represent the significant mantle contribution in the Heunghae and Yeonil areas. Through the distribution of high $^3He/^4He$ ratios, we propose that the Heunghae, Namsong, and Jamyeong faults are the passage of mantle-derived fluids. Computed ^3He fluxes of the Heunghae (120 to 3,000 atoms cm^{-2} sec^{-1}), Namsong (52 to 1,300 atoms cm^{-2} sec^{-1}), and Jamyeong (83 to 2,100 atoms cm^{-2} sec^{-1}) faults are comparable to other major active faults around the world, reflecting either high porosity or high helium flow rates. Therefore, our results demonstrate that there are active faults near the EGS facilities, which can provide the basis for future studies.

1. Introduction

Enhanced geothermal system (EGS) is a type of heat exchanger designed to improve the efficiency of geothermal energy plants. EGS is configured to enable convective production or to improve heat production. One of the main goals of EGS is to increase the permeability of reservoir rocks with high temperatures but low permeability. For this purpose, hydraulic fracturing, fluid injection (and/or extraction), and acidification can be used [1].

The correlation between EGS and seismic activity has been proposed for decades [1]. Geysers (USA), Cooper Basin (Australia), Berlin (El Salvador), Soultz-Sous-Forêts (France), and Basel (Switzerland) are well-known examples of EGS-related earthquake activities. In addition to these cases at the EGS site, for other cases such as wastewater injection, carbon capture and storage (CCS), or hydrocarbon (e.g., shale gas and oil) extraction, fluid injection, and hydraulic fracturing are often proposed as triggers of earthquakes (e.g., Keranen et al. [2]). Two mechanisms for triggering earthquakes associated with fluid injection and/or extraction are described by McGarr et al. [3]; (1) direct fluid pressure effects on injection and (2) changes in solid stress due to fluid extraction and/or injection. As we can infer from

earthquake-inducing mechanisms of fluid injection, knowing locations of faults around the EGS site is important for society. For both cases, it is necessary to identify not only faults beneath the EGS site but also any potentially unknown faults. In the case of the 2019 Ridgecrest earthquake, for example, it shows how the earthquake swarm can propagate to interlocked faults [4]. This refers to the possibilities that the small induced earthquake can trigger much larger seismicity than expected, which amplifies the seismic hazards and risks around the EGS site.

Since mantle-derived fluids have been identified and quantified from the San Andreas Fault system [5] in the nonvolcanic region, noble gas studies have been conducted in several active fault zones to understand the fluid behavior related to seismicity (e.g., Sano et al. [6]). Even in some cases, helium isotope ratio distribution could detect concealed fault zones [7]. Noble gases and their isotope compositions can be used as natural tracers. They are chemically inert, retaining their properties through the water-rock systems. Therefore, the contents and isotopic compositions of noble gases allow us to trace the fluid sources into mantle, crust, and atmosphere. It is also possible to quantify the contribution of each source [8]. Mantle-derived helium and CO_2 degassing through faults in the southeastern Korean peninsula has recently been reported [9].

Here, we report new chemical and isotopic compositions of dissolved gases in groundwater, which are rarely been documented in the study area. Then, we will first discuss the general characteristics of gas compositions in this area. Based on the results, the perceptual impact on the composition of the noble gas is assessed to suggest that there are active fault zones near the EGS site, reaching the upper mantle through continental crust. In addition, helium flux through faults was calculated and compared with the characteristics of major fault zones around the world.

1.1. Geological Setting. The Pohang region consists of three subdivisions: Heunghae, Yeonil, and Sinkwang areas (Figure 1). The Heunghae and Yeonil areas are located in Pohang Basin, the Miocene sedimentary basin, and the Sinkwang area is near the Yangsan fault (Figure 1). Pohang Basin is one of the largest sedimentary basins in the Korean Peninsula [10]. The border faults in Pohang Basin are the Yeonil tectonic line, the Ocheon fault system, and segmented faults bounding to the west (Figure 1). These western boundary segment faults are almost parallel to the Yangsan fault, 2-7 km away from the west. During the early Miocene period, Pohang Basin was formed while the East Sea (Sea of Japan) which is a back-arc basin was opened, and the opening was ceased at ~15 Ma [11, 12]. The sedimentation in the Pohang Basin lasted from 17 to 10 Ma [11, 12]. The basin is filled with Paleogene volcanic rocks and granite, followed by Neogene conglomerates, sandstone, and mudstone, with a total thickness of less than 500 m [13, 14]. The basin has been cut by normal faults with the NNE-SSW strike and eastern dip. These normal faults have been formed after 15 Ma, blocked by other normal faults with the ENE-WSW strike [14]. The Sinkwang area is spread over Cretaceous biotite granite cut by the Yangsan fault covered with quaternary sediments (Figure 1, [14]). The Yangsan fault, located at the current Cretaceous sedimentary area, is a strike-slip fault formed in the early Cretaceous period as a result of tension due to the subduction of the Izanagi plate [15, 16]. After the subduction of the Pacific plate in the late Cretaceous period, compressive stresses affected the Yangsan fault. The direction of compressive stress was initially in the NW-SE direction at the end of the Cretaceous period, and the direction of subduction at the end of the Paleogene changed and moved in the NE-SW direction [15, 16].

1.2. 2017 Pohang Earthquake. The Pohang enhanced geothermal system (EGS) project was launched in November 2010 to produce 160°C geothermal water and 1.2 MW geothermal energy in a nonvolcanic area [17]. To construct the EGS facility, two boreholes (PX-1 and PX-2) were drilled through the sedimentary basin into the granodiorite basement rock. The measuring depths of the two boreholes (MD, measured along the borehole) are 4,362 m and 4,382 m, respectively. Hydraulic fracturing and fluid injection were performed from January 2016 to September 2017 to increase geothermal productivity [17]. During this period, five hydraulic stimuli were performed through PX-1 and PX-2. First, the third and fifth hydraulic stimuli were performed on the PX-2 with maximum well-head pressures of 89.2 MPa, 88.8 MPa, and 84.6 MPa, respectively. The second and fourth hydraulic stimuli were performed on the PX-1, and the maximum well-head pressures were 27.71 MPa and 25.16 MPa, respectively.

After the third hydraulic stimulation, an earthquake occurred with Mw 3.2. About two months after the cessation of the fifth hydraulic stimulus, on November 15, 2017, an earthquake with Mw 5.5 occurred (Figure 1), followed by more than one hundred aftershocks (≥ Mw 2.0). The earthquake was the second-largest earthquake in the Korean Peninsula since modern earthquake observation has begun in 1978, resulting in physical and economic damage to local residents (135 people were injured and more than 1,700 people were in emergency housing; directly USD 75 M and total economic impact USD 300 M) [17]. Due to this great impact on Korean society, it is necessary to study active faults related to potential seismic crises in this area.

2. Methods

We collected groundwater samples from groundwater wells in the Heunghae, Yeonil, and Sinkwang areas, Pohang, Republic of Korea (Table 1, Figure 1). Ranges of water temperatures and pH are 14.3 to 20.5°C and 6.0 to 9.0, respectively, and well depth ranges between 30 and 230 m from the topographic surface. The samples were stored in copper tubes and sealed with clamps, except for PH-3 that was collected in a preevacuated Giggenbach bottle. Dissolved gases were extracted from water samples by the high vacuum system and analyzed in the Atmosphere and Ocean Research Institute (AORI), the University of Tokyo. Concentrations (consist of CO_2, N_2, O_2, CH_4, Ar, and He) of dissolved gases were measured by a Pfeiffer QMS 200 quadrupole mass spectrometer (QMS).

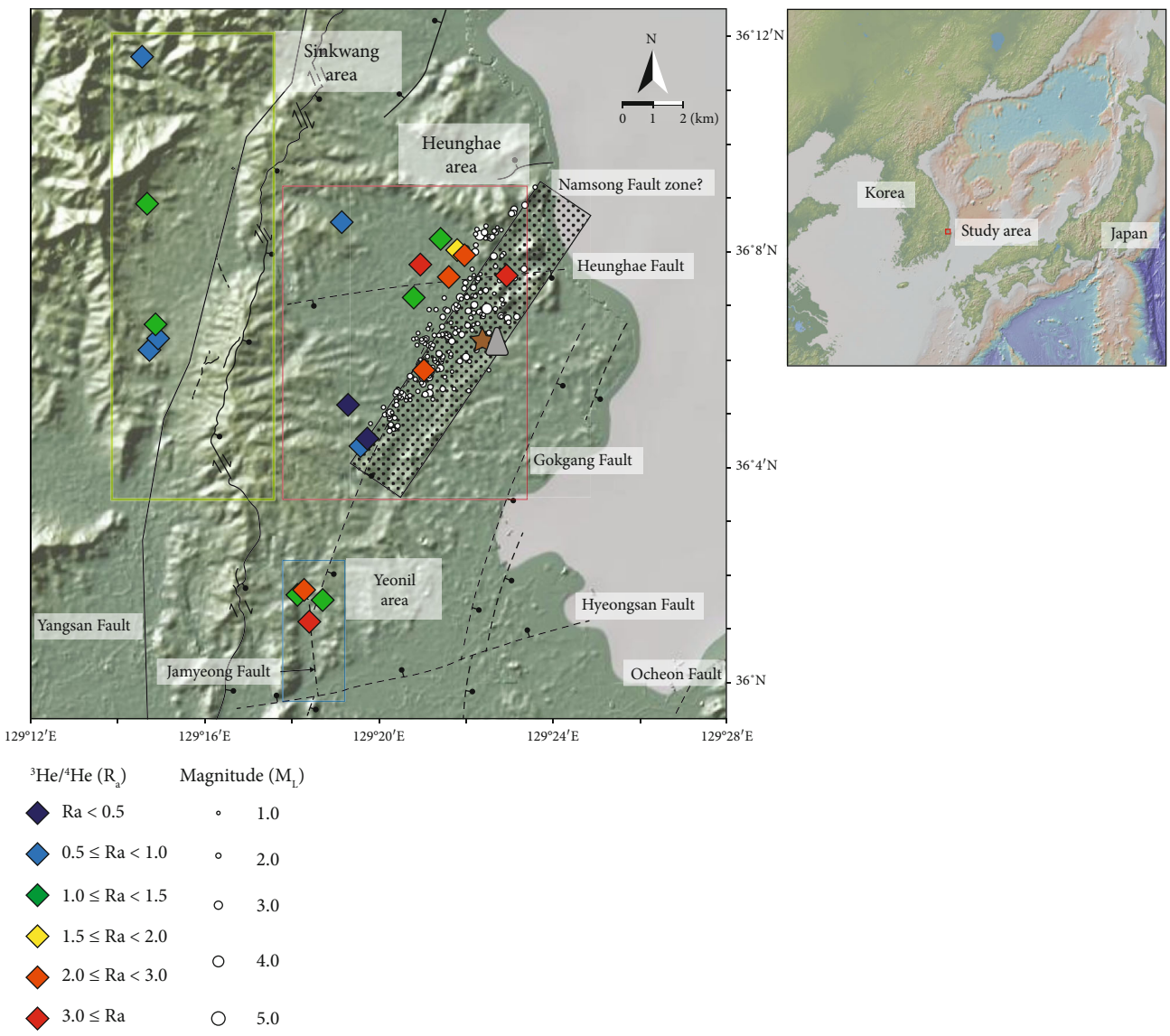

Figure 1: Geological map of Pohang, South Korea (modified from Song [14]), created by GeoMapApp 3. 6. 10 [52]. Sample locations are marked with diamond symbols. Each symbol is represented by a helium isotope ratio ($^3He/^4He$). The location and scale (white circle) of aftershocks until 2017 are excerpts from the 2017 annual report of earthquakes published by the Korea Meteorological Agency (KMA). The gray triangle represents the EGS site, and the brown star stands for the epicenter of the Mw 5.5 earthquake that occurred on November 15, 2017.

Stable isotope compositions of nitrogen for N_2 and carbon for CO_2 and CH_4 were measured by an isotope ratio mass spectrometer (Isoprime 100 by Elementar). For samples with high CH_4 concentration (>4%), coexisting CO_2 and CH_4 were separated before measurement by liquid nitrogen. To measure $^3He/^4He$ and $^4He/^{20}Ne$ ratios, dissolved gas samples were purified by titanium getters at 400°C and charcoal traps at liquid nitrogen temperature. Neon was trapped by the cryogenic pump at 40 K after measuring $^4He/^{20}Ne$ ratios via online QMS (Pfeiffer Prisma 80). Then, purified helium was injected into a noble gas mass spectrometer (Helix SFT by ThermoFisher) to measure $^3He/^4He$ ratios. Calibration of He isotope ratios was conducted by using the internal He standard of Japan (HESJ) [18]. Measured $^3He/^4He$ ratios were corrected for atmospheric helium by using measured $^4He/^{20}Ne$ ratios, since ^{20}Ne is assumed to be mostly atmospheric [19]. From Sano et al. [20]:

$$\frac{Rc}{Ra} = \left[\left(^3He/^4He\right)_{measured} - r\right]/(1-r)$$
$$r = \left(^4He/^{20}Ne\right)_{ASW}/\left(^4He/^{20}Ne\right)_{measured} \quad (1)$$

where Rc/Ra is the corrected $^3He/^4He$ ratio, and $(^4He/^{20}Ne)_{ASW}$ is the $^4He/^{20}Ne$ ratio of air-saturated water (ASW). Analytical errors for and $^3He/^4He$ and $^4He/^{20}Ne$ ratios are about 1% and 5% (1σ), respectively.

Table 1: Sampling information, gas composition, and ratios of the main components of the Pohang samples.

ID	Region	Latitude	Longitude	Date	Type	T	pH	Well depth	He	CH_4	N_2	O_2	Ar	CO_2	He/Ar	N_2/Ar	N_2/He
		°N	°E			°C		m	ppm	(vol.%)							
P-11	Heunghae	36.08608	129.321591	2019-02-21	Groundwater	15.4	8.5	120	104	0.2	94.0	—	2.1	4.1	0.005	45	9,041
P-12		36.12613	129.382112	2019-02-20	Groundwater	14.3	7.3	154	215	0.6	88.1	2.0	1.7	7.6	0.01	53	4,099
P-14		36.12574	129.360214	2019-02-20	Groundwater	16.4	7.2	110	170	36.7	32.5	0.2	0.6	30.0	0.03	51	1,909
DS-1		36.14254	129.319276	2019-02-21	Groundwater	15.4	7.9	120	279	—	63.5	—	1.3	36.6	0.02	50	2,277
PH19-01		36.11937	129.346867	2019-04-11	Groundwater	18.0	7.0	130	9	3.8	73.0	—	1.6	22.0	0.001	46	81,078
PH19-03		36.13743	129.357115	2019-04-12	Groundwater	16.5	6.0	30	14	0.2	53.8	—	1.1	45.4	0.001	51	38,400
PH19-04		36.13393	129.36331	2019-04-12	Groundwater	19.1	7.0	150	44	0.6	76.3	—	1.3	22.0	0.003	57	17,332
PH19-05		36.13235	129.366165	2019-04-12	Groundwater	17.7	7.0	150	101	1.3	61.8	—	1.3	35.7	0.01	49	6,114
PH19-06		36.12957	129.349261	2019-04-12	Groundwater	17.1	7.0	78	468	0.4	66.2	1.4	1.5	30.5	0.03	45	1,414
PH19-10		36.07346	129.326287	2019-04-13	Groundwater	15.9	7.0	120	12	0.6	62.9	—	1.4	35.6	0.001	46	52,442
PH19-11		36.07565	129.32894	2019-04-13	Groundwater	16.8	7.0	120	43	0.1	77.7	—	1.6	21.0	0.003	48	18,063
PH19-12		36.09678	129.350515	2019-04-13	Groundwater	17.3	6.0	230	701	18.7	47.5	—	1.0	33.1	0.07	49	678
PH19-07	Yeonil	36.01893	129.306846	2019-04-13	Groundwater	20.5	8.0	160	2744	34.3	57.9	—	0.9	6.9	0.3	64	211
PH19-08		36.02889	129.304796	2019-04-13	Groundwater	20.2	8.0	160	597	42.9	48.1	—	0.9	8.3	0.1	55	806
PH19-09		36.02730	129.302284	2019-04-13	Groundwater	16.1	7.0	—	7	0.1	75.2	—	1.6	23.4	0.0004	46	107,400
PH-3		36.02572	129.311889	2018-11-17	Groundwater	17.0	9.0	101	8	31.0	60.0	8.0	0.9	0.1	0.001	67	74,988
P-2	Sinkwang	36.10668	129.248979	2019-02-20	Groundwater	15.4	7.1	120	16	0.1	84.2	—	1.3	14.7	0.001	67	52,631
P-3		36.19378	129.242729	2019-02-20	Groundwater	15.2	7.4	210	16	0.1	74.6	—	1.6	24.3	0.001	48	46,613
P-4		36.10299	129.245568	2019-02-20	Groundwater	15.0	6.6	88	11	0.1	69.3	0.8	1.3	28.5	0.001	53	63,000
P-5		36.11097	129.247894	2019-02-20	Groundwater	14.8	7.1	120	32	—	60.8	—	1.2	41.4	0.003	51	19,009
P-7		36.14834	129.244634	2019-02-20	Groundwater	16.0	6.5	178	14	0.1	61.5	—	1.2	37.8	0.001	52	43,921

3. Results

The measured gas compositions are reported in Table 1. N_2 is the most abundant gas component for most samples with the range of 32.5 to 94.0 vol.%. CO_2 is also observed in all samples ranging from 0.1 to 45.4 vol.%. CH_4 is also one of the main components for samples in the Heunghae and Yeonil areas (for example, P-14, PH19-12, PH19-07, PH19-08, and PH-3) with the range from 18.7 to 42.9 vol.%. Ar and He range from 0.6 to 2.1 vol.% and from 7 to 2744 ppm, respectively. Except for PH-3 (O_2 = 8.0 vol.%), almost no O_2 is observed in most samples, indicating minimum air contamination during sampling and analysis. Isotopic compositions of N, C, and He are summarized in Table 2. The nitrogen isotope compositions of N_2 ($\delta^{15}N$-N_2) for all samples range from 0.19 to 3.56‰, all heavier than air (0‰). Carbon isotope values of CO_2 ($\delta^{13}C$-CO_2) for all samples range from -27.33 to -16.01‰. There is no significant regional difference for $\delta^{15}N$-N_2 and $\delta^{13}C$-CO_2. The carbon isotope composition of CH_4 ($\delta^{13}C$-CH_4) is from -76.05 to -70.04‰, implying similar CH_4 sources for both Heunghae and Yeonil areas. In these areas, most samples show $^4He/^{20}Ne$ ratios higher than ASW ($^4He/^{20}Ne = 0.268$, [21]), with $^3He/^4He$ ratios ranging from 0.18 to 3.83 Ra, where Ra is the $^3He/^4He$ ratio of air (1.4×10^{-6}, [22]). The $^3He/^4He$ ratios (0.90 to 1.22 Ra) of the Sinkwang groundwater samples are atmospheric because $^4He/^{20}Ne$ ratios of the samples are similar to air.

4. Discussion

4.1. Gas Geochemistry. Based on the N_2-Ar-He ternary diagram (Figure 2), nonreactive gases (N_2, Ar, and He) in the Heunghae and Yeonil areas display a two-component mixing relationship between the mantle and atmospheric end members. Lee et al. [9] have shown that fault gases in the southeastern Korean peninsula are continental gases rather than subduction zone gases. Dissolved gases in groundwater from the Sinkwang area are atmospheric with low He/Ar ratios (0.003 to 0.001). Lee et al. [9] addressed that some gas samples which are severely contaminated by air in southeastern Korea are due to shallow well depths (130 to 296 m). However, in the Heunghae and Yeonil areas, it is unlikely that well depths (Table 1) and contribution from deeply derived gases are relevant. Instead, we suggest that distance to the permeable fault zones where gases released from deep sources are transported is important. In general, groundwater wells in the Heunghae and Yeonil areas contain more dissolved helium (Table 2), implying there are more permeable areas than the Sinkwang area.

CO_2 concentrations are negatively correlated with pH ($R^2 = 0.62$), indicating that CO_2 is likely to be trapped in high pH water to be present as HCO_3^- and CO_3^{2-} (Figure S1a, [23, 24]). To verify this, we show that CO_2/N_2 ($R^2 = 0.61$) and CO_2/CH_4 ($R^2 = 0.41$) ratios also have negative trends with pH (Figure S1b, c). It is attributable that CO_2 removal increased those ratios because N_2 and CH_4 are not responsive to pH changes. Also, N_2 and/or CH_4-rich gases are found in alkaline springs [23, 25, 26]. Moreover, CO_2/CH_4 ratios and helium concentrations show a negative correlation ($R^2 = 0.76$, Figure S1d). Although Lee et al. [9] suggested both CO_2 and helium are derived from the mantle source in southeastern Korea, it is plausible that their origins are decoupled in the Pohang region.

4.2. Origins of Nitrogen, Carbon Dioxide, and Methane. $\delta^{15}N$-N_2 values of all samples with the range of 0.19 to 3.56‰ are between the air (0‰) and sediment (7‰) end-members. By plotting $\delta^{15}N$ with $N_2/^3He$ ratios (Figure 3(a)), we can identify contributions of the air, sediment, and mantle end-members. To quantify the contribution of each end-member, we adopted the three-component mixing model from Sano et al. [27]:

$$\delta^{15}N_{obs} = f_M \times \delta^{15}N_{mantle} + f_S \times \delta^{15}N_{sediment} + f_A \times \delta^{15}N_{air}$$
$$\frac{1}{(N_2/^3He)_{obs}} = \frac{f_M}{(N_2/^3He)_{mantle}} + \frac{f_S}{(N_2/^3He)_{sendiment}} + \frac{f_A}{(N_2/^3He)_{air}}$$
$$f_M + f_S + f_A = 1 \quad (2)$$

where obs is the observed value; f_M, f_S, and f_A are the contributions of the mantle, sediments, and air; $\delta^{15}N_{mantle}$, $\delta^{15}N_{sediment}$, and $\delta^{15}N_{air}$ are -5 ± 2‰, 7 ± 4‰, and 0‰; $N_2/^3He_{mantle}$, $N_2/^3He_{sediment}$, and $N_2/^3He_{air}$ are 8.9×10^5, 1.4×10^{12}, and 1.1×10^{11}, respectively [21, 27, 28, 29 and references therein]. The results are summarized in Table S1. Air is the most dominant source for N_2 in the Pohang region with the f_A range of 49.1 to 97.0%. Also, sediment is another main source for N_2 with the f_S range of 2.8 to 50.9%. The mantle contribution is very minor (f_M = 0 to 1.0%), indicating N_2 is the primarily sedimentary origin and is contributed by air at shallow depths. Moreover, the sediment-derived N_2 in the Pohang region is of shallow origin rather than the recycled nitrogen through subduction as discussed in section 4.1.

The Pohang region has no mantle-derived CO_2 which has been reported in Gyeongju and Ulsan areas, southeastern Korea (Lee et al., 2019). $\delta^{13}C$ values (-27.33 to -16.01‰) of CO_2 in all samples are lighter than the MORB value (-6.5 ± 2.5‰, [30]) and lie approximately between the mean $\delta^{13}C$-CO_2 values of C3 (-27‰) and C4 (-13‰) plants [31] (Figure 3(b)). The results are similar to those of most fault gases previously reported in southeastern Korea ($\delta^{13}C - CO_2 = -14.50$ to -24.92‰) as well as $\delta^{13}C$-CO_2 values (-11.9 to -24.0‰) in global fault zones without magma activity, such as San Andreas Fault and North Anatolian Fault [9 and references therein]. On the $\delta^{13}C$-CO_2 vs $CO_2/^3He$ plot (Figure S2), a majority of samples are outside the mixing curve between the biogenic and mantle end-members due to their low $CO_2/^3He$ ratios. As discussed in section 4.1, the decrease in $CO_2/^3He$ ratios can be attributed to CO_2 loss in this area under the influence of pH. Moreover, the negative correlation ($R^2 = 0.88$) between ^4He concentrations and $CO_2/^3He$ ratios is displayed well (Figure S1e). Gilfillan et al. [32] have shown the same trend for natural gas fields in North America. They argued that

Table 2: Analysis of stable isotopes and noble gases in the Pohang area.

ID	Area	$^3He/^4He$	Error	$^3He/^4He$	$^4He/^{20}Ne$	$^{20}Ne/^4He$	^4He	^{20}Ne	$\delta^{15}N$	Error	$N_2/^3He$	$\delta^{13}C$	Error	$CO_2/^3He$	$\delta^{13}C$	Error	$CH^4/^3He$
		R/Ra		**Rc/Ra**			**ccSTP/g**	**ccSTP/g**	**N_2**	**(1σ)**		**CO_2**	**(1σ)**		**CH_4**	**(1σ)**	
P-11	Heunghae	0.18	0.02	0.05	1.8	0.6	4.06.E-07	2.22.E-07	2.15	0.48	3.52E+10			1.53E+09			8.98E+07
P-12		3.83	0.01	3.92	7.7	0.1	1.91.E-06	2.48.E-07	3.15	0.35	7.70E+08	-19.49	0.31	6.64E+07			5.59E+06
P-14		2.69	0.01	2.71	21.4	0.1	2.66.E-06	1.24.E-07	3.16	0.53	5.11E+08	-19.49	0.31	4.72E+08	-70.04	0.41	5.78E+08
DS-1		0.87	0.02	0.80	0.7	1.4	1.65.E-07	2.37.E-07	2.43	0.28	1.89E+09	-27.33	0.6	1.09E+09			—
PH19-01		1.30	0.01	1.38	1.2	0.9	2.04.E-07	1.75.E-07	3.12	0.3	4.55E+10	-16.01	0.35	1.37E+10			2.38E+09
PH19-03		1.35	0.01	2.57	0.3	3.1	8.59.E-08	2.67.E-07	2.62	0.3	2.03E+10	-23.08	0.31	1.71E+10			6.78E+07
PH19-04		1.99	0.01	2.12	2.2	0.5	2.99.E-07	1.38.E-07	2.42	0.26	6.21E+09	-25.29	0.32	1.79E+09			5.05E+07
PH19-05		2.49	0.01	2.54	7.1	0.1	1.32.E-06	1.87.E-07	0.96	0.25	1.77E+09	-25.77	0.31	1.02E+09			3.83E+07
PH19-06		3.38	0.01	3.45	8.9	0.1	1.75.E-06	1.98.E-07	1.80	0.25	3.02E+08	-23.14	0.37	1.39E+08			1.87E+06
PH19-10		0.79	0.01	0.29	0.4	2.8	7.22.E-08	2.03.E-07	1.78	0.27	4.99E+10	-20.78	0.32	2.82E+10			4.92E+08
PH19-11		0.36	0.02	0.06	0.8	1.3	1.58.E-07	2.01.E-07	1.25	0.22	3.60E+10	-20.66	0.38	9.74E+09			5.10E+07
PH19-12		2.25	0.01	2.26	61.9	0.02	6.84.E-06	1.11.E-07	1.57	0.26	2.17E+08	-25.71	0.3	1.51E+08	-76.05	0.47	8.51E+07
PH19-07	Yeonil	3.09	0.01	3.09	145.3	0.01	1.07.E-05	7.35.E-08	1.26	0.24	4.92E+07	-21.66	0.34	5.88E+06	-75.40	0.35	2.91E+07
PH19-08		2.32	0.01	2.33	61.9	0.02	6.96.E-06	1.12.E-07	0.19	0.23	2.50E+08	-23.70	0.46	4.32E+07	-75.13	0.33	2.23E+08
PH19-09		1.00	0.01	1.00	0.4	2.8	4.83.E-08	1.36.E-07	2.06	0.24	7.60E+10	-20.09	0.34	2.36E+10			6.06E+07
PH-3		1.26	0.03	1.31	1.5	1.3			0.33	0.01	4.07E+10			8.81E+07	-71.47	0.1	2.10E+10
P-2	Sinkwang	0.90	0.02	0.33	0.3	3.4	1.21.E-07	4.11.E-07	1.44	0.21	4.21E+10	-26.31	0.41	7.35E+09			3.00E+07
P-3		0.91	0.01	0.70	0.4	2.8	7.35.E-08	2.07.E-07	3.56	0.36	3.66E+10	-26.69	0.47	1.19E+10			2.45E+07
P-4		0.96	0.02	0.86	0.4	2.8	8.41.E-08	2.37.E-07	1.21	0.22	4.54E+10	-25.43	0.36	1.87E+10			3.28E+07
P-5		1.09	0.01	1.51	0.3	3.3	7.74.E-08	2.55.E-07	3.07	0.27	1.27E+10	-25.57	0.38	8.62E+09			—
P-7		1.22	0.01	2.30	0.3	3.3	1.35.E-07	4.47.E-07	1.91	0.29	2.57E+10	-23.86	0.32	1.58E+10			2.09E+07

Note: the standards for $\delta^{15}N$ and $\delta^{13}C$ are air and Pee Dee Belemnite (PDB), respectively. Concentrations of ^4He and ^{20}Ne of PH-3 were not measured because the sampling method was different. The carbon isotope ratios of CO_2 in P-11 and PH-3 were not measured due to their low concentrations.

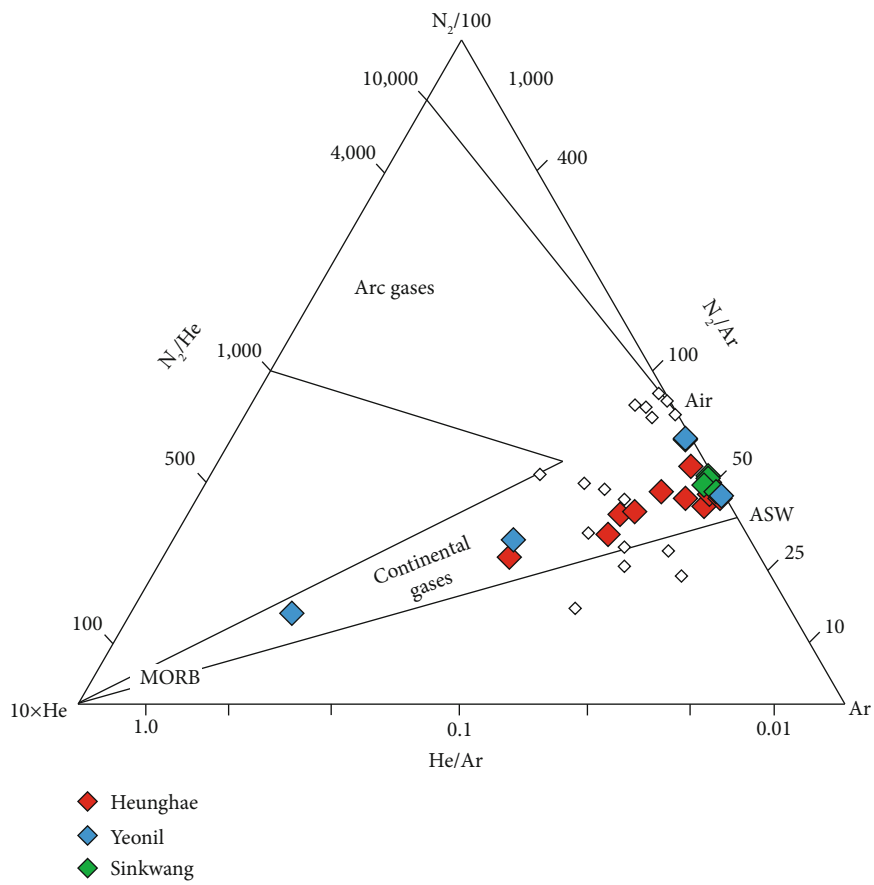

Figure 2: N_2-Ar-He ternary plot. Reference data of fault-related gas samples in the southeastern part of the Korean peninsula (white diamond) is shown [9]. All samples are mixed between MORB, air, and air-saturated water (ASW) and displayed as the trend of continental gas.

noble gases are unlikely involved in increasing or decreasing $CO_2/^3He$ ratios. However, the trend between $^3He/^4He$ and $CO_2/^3He$ ratios (Figure S1f) is also negatively correlated ($R^2 = 0.54$). Thus, in the Pohang region, we argue that not only CO_2 loss but also external helium was introduced to reduce $CO_2/^3He$ ratios in the local groundwater layer (see section 4.3-4.5). This further supports that CO_2 source derived from shallower sediments than the mantle.

The origin of CH_4 in Pohang is relatively uniform. In the measured samples (Table 2), $\delta^{13}C$ values of CH_4 range from -76.05 to -70.04‰, indicating a typical microbial origin [33]. Considering $\delta^{13}C$ of CO_2, the mechanism of production of CH_4 is resulted by carbonate reduction with slight oxidation after the process of methanogenesis (Figure S2b, [34]). Therefore, the isotope separation factors ($\varepsilon_C CO_2$-CH_4) which are approximately from 54.36 to 58.12 allow us to estimate the growth temperature of CH_4 at ~40°C [34].

4.3. Helium Isotope Geochemistry in the Pohang Area. In the Pohang region, higher $^3He/^4He$ ratios (up to 3.83 Ra) than ASW/air are found in the Heunghae and Yeonil areas. Although elevated $^3He/^4He$ ratios can be resulted by the ^3H-derived ^3He, it is unlikely because the samples with high $^3He/^4He$ ratios also have high $^4He/^{20}Ne$ ratios (up to 145.29). Helium is also remobilized from old igneous rocks [35]. It is known that Pohang Basin is filled by sediments on the granodiorite basement rocks with some Tertiary basaltic rocks (Daljeon basalt) which erupted at 13.8 Ma [14 and references therein]. However, the basaltic rocks show a limited distribution (<1 km^2) in the Yeonil area [14 and references therein]. Considering the typical ^4He contents in inclusion bearing olivine (10^{-8} to 10^{-9} ccSTP/g, [8, 35]) and the ^4He concentrations of high $^3He/^4He$ ratio samples from the Yeonil area (1.1×10^{-5} to 7.0×10^{-7} ccSTP/g), the amounts of trapped ^3He in the Daljeon basalt is insufficient to be the source of ^3He in the Yeonil area. Furthermore, in consideration of general Li concentration of igneous and sedimentary rock, radiogenic ^3He by decay reaction $^6Li(n, \alpha)^3H(\beta\text{-})^3He$ cannot affect $^3He/^4He$ ratio of groundwater [35 and references therein]. Therefore, the excess ^3He in the Pohang region originates from the mantle as well as ^4He [23, 36].

The range of $^3He/^4He$ ratios (0.18 to 3.83 Ra) in the Heunghae area is wide, indicating that both mantle and crustal helium sources are present in a short range, up to 10 km (Figures 1 and 4). Even though some samples (PH19-09 and PH-3) in the Yeonil area are atmospheric (Figures 1 and 4), two samples (PH19-07 and PH19-08)

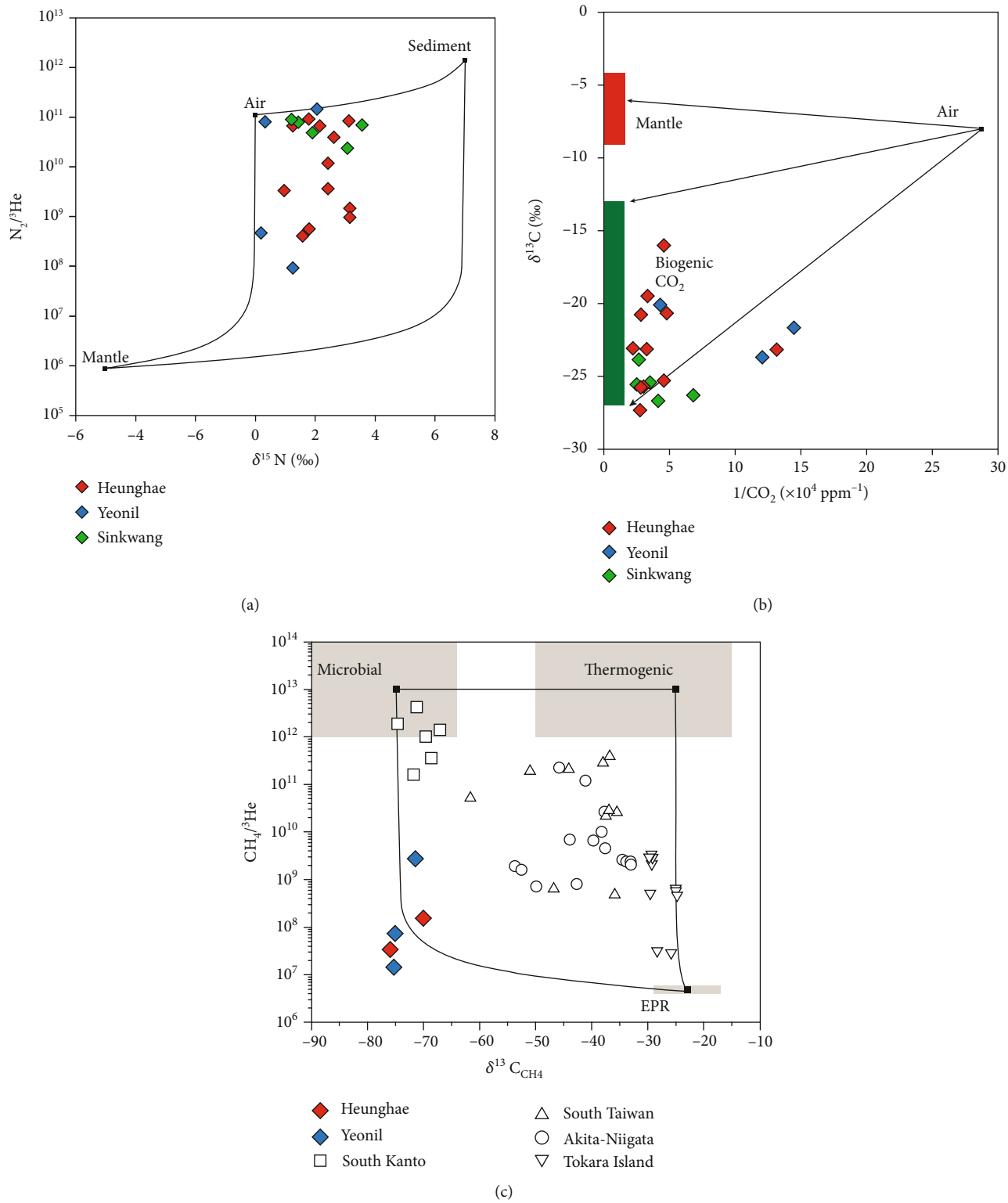

Figure 3: (a) $N_2/^3He$ versus $\delta^{15}N$ diagram. Each end-member and mixing lines are described in section 4.2. (b) $\delta^{13}C$ of CO_2 versus $1/CO_2$ diagram (modified from Lee et al. [53]). Mantle value of $\delta^{13}C$ (-6.5 ± 2.5‰) is from Sano and Marty [30]. The biogenic CO_2 area ranges between $\delta^{13}C$ values of C3 plant and C4 plant [31]. The air value of $\delta^{13}C$ and CO_2 concentration are from Lewicki and Brantley [54]. (c) $CH_4/^3He$ versus $\delta^{13}C$ of CH_4 diagram (modified from Sano et al. [55]). Reference data from northeastern Asia is shown together (Sano et al. [55]).

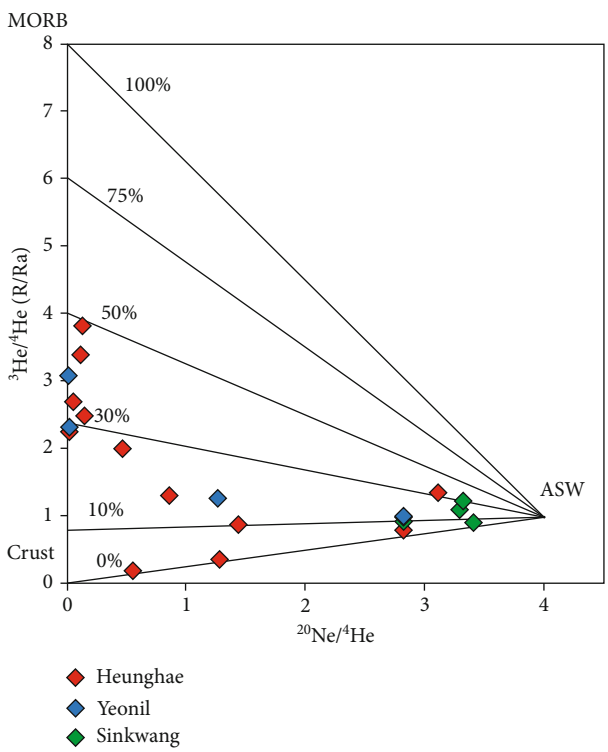

Figure 4: ^{3}He/^{4}He versus ^{20}Ne/^{22}Ne diagram. The reference values for MORB, ASW, and Crust are shown. Each line represents mixing lines between ASW and external helium sources with different MORB contributions.

have high ^{3}He/^{4}He (3.09 Ra and 2.32 Ra) and ^{4}He/^{20}Ne (145.29 and 61.86) ratios, implying the presence of mantle-derived fluids. All samples in the Sinkwang area show atmospheric ^{3}He/^{4}He (0.90-1.34 Ra) and ^{4}He/^{20}Ne (0.27-0.36) ratios (Figures 1 and 4). A ^{3}He/^{4}He ratio of up to 5.69 Ra was reported for the Yangsan fault zones [9]. The absence of mantle signatures for all samples in the Sinkwang area can be explained by the distance from the main fault line (Figure 1), which means the influx of external helium is quite low.

The highest ^{3}He/^{4}He ratio (3.83 Ra) represents about 50% of the mantle contribution to the fluid (Figure 4). It is known that mantle-derived helium can be actively released to the surface through magmatism [37, 38]. However, the Pohang region is located hundreds of kilometers away from the active volcanoes of the Japanese arc (Figure 1). A low-velocity zone beneath Ulleungdo has been proposed by Chen et al. [39] and references therein, which is also 200 km away from Pohang. Moreover, magma activity in this area has been ceased after 9,300~6,300 BP [40 and references therein].

The appropriate model for the occurrence of mantle-derived helium in this region is that there are permeable fault zones like the release of mantle fluids in the San Andreas Fault zones [5]. According to Song [14], there are some faults in the Pohang region, such as Heunghae, Gokgang, Hyeongsan, and Ocheon faults (Figure 1). Also, Westaway and Burnside [41] named the new fault as the Namsong fault on the basis of the aftershock distribution of the Pohang earthquake (Figure 1) and proposed that the fault has been already critically stressed before the EGS project [41]. In addition, according to the Korea Meteorological Administration (KMA), the depths of the 2017 Pohang earthquake and aftershocks are less than 16 km, which is shallower than the Moho depth (~28 km) of the region [42]. Kennedy and Van Soest [37] suggested that the mantle fluids of the San Andreas Fault penetrate the brittle-ductile boundary based on helium isotope ratios and strain rates measured by GPS. To explain the mantle-derived helium in the Gyeongju and Ulsan areas, southeastern Korea, Lee et al. [9] also proposed that mantle helium migrates along the ductile shear zone underneath the brittle regime.

From the above information, in the Pohang region, we suggest that there have been already tectonically active areas that have developed from the ductile shear zone to the brittle fault zone. This condition enabled the inflow of the mantle-derived fluids through the lower crust into the permeable faults. Furthermore, in this area, relatively high temperatures, heat contents, and heat flows have been reported [43 and references therein], supporting that ^{3}He came from the mantle through active faults (e.g., Umeda et al. [44]).

4.4. Distribution of Active Faults. As discussed in section 4.3, we identified the existence of permeable faults in the Heunghae and Yeonil areas. The locations of the faults can be constrained based on the geographical distribution of helium isotope ratios [7]. Since the latitude variation in the ^{3}He/^{4}He ratios is the most prominent to specify fault locations, we can show the relationship between the ^{3}He/^{4}He ratios and latitude (Figure S3). Although it is known that the location of the Heunghae fault is still ambiguous, we found that the distribution of higher ^{3}He/^{4}He ratios are well consistent with the fault striking EW at 36.126°N (Figure 1). Also, there is a relationship between higher ^{3}He/^{4}He ratios and distance from the fault line (Figure 5(a)), which has been observed in the San Andreas, North Anatolian, and Karakoram faults [5, 8, 37, 45]. In Figure 5(a), we could observe a sample (PH19-12) with a high ^{3}He/^{4}He ratio (2.25 Ra), which is about 3 km away from the Heunghae fault to the south (Figures 1, S3). The sampling location of PH19-12 is still in the area where aftershocks have frequently occurred (Figure 1), suggesting there can be another ^{3}He discharge in the Heunghae area. To confirm the pathway of mantle-derived helium, we calculated the distance of all samples from the Namsong fault (Figure 5(b)). Based on the mainshock strike (N34°E) and dip (51°NW), we assumed that the easternmost boundary of the aftershock occurrences (from 2017 Annual report of Earthquake) with the N34°E strike is the uppermost line of the fault. By using this uppermost line, the distance from the closest fault and ^{3}He/^{4}He ratios are displayed (Figure 5(c)), showing a better correlation with exponential distribution ($R^2 = 0.80$) than Figure 5(a). To validate the relationship between the distance from faults and ^{3}He/^{4}He ratios, we selected six samples at latitudes higher than P12 (Figure 5(a), red circles). These samples are well correlated with distance from the Heunghae fault exponentially ($R^2 = 0.98$), validating the model of the Heunghae-

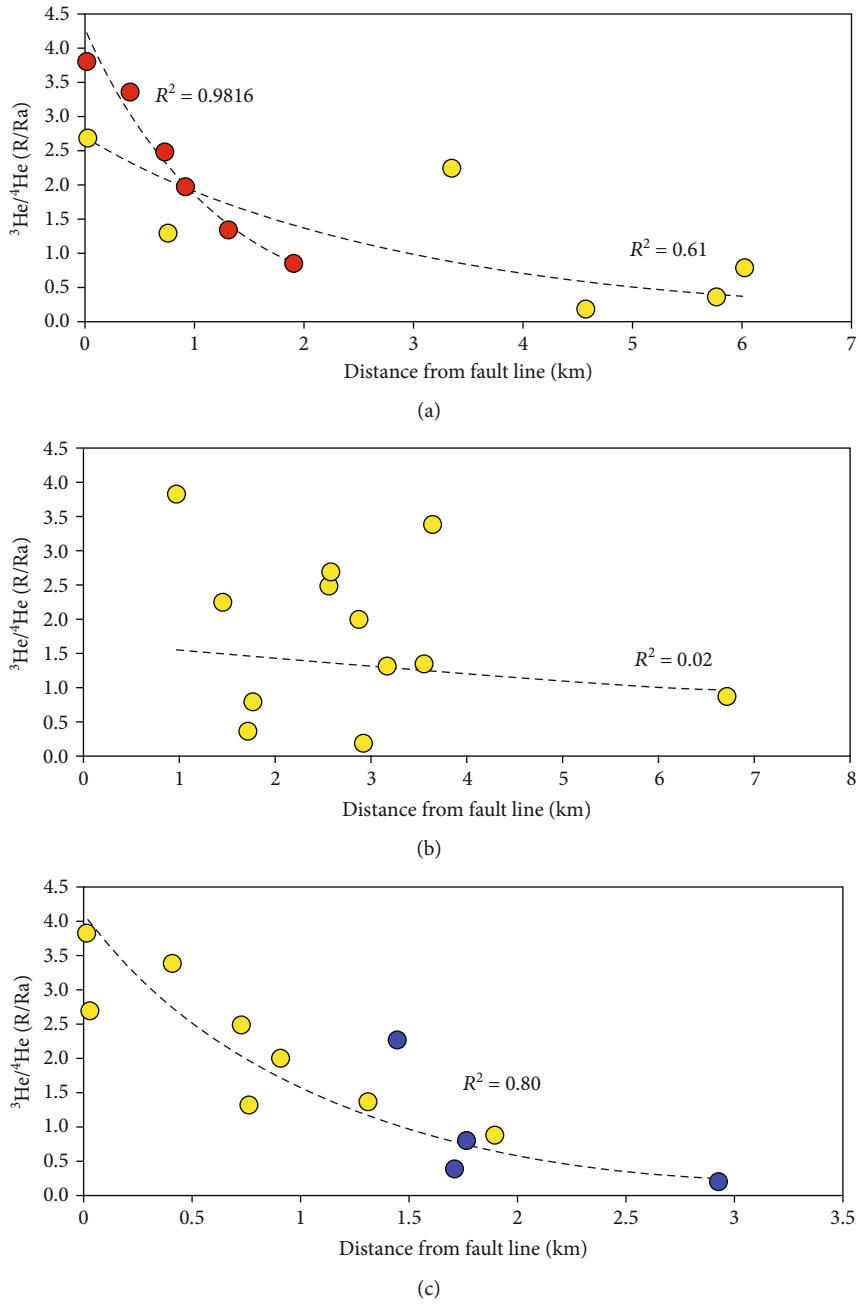

Figure 5: (a) ^{3}He/^{4}He ratios to distance from the Heunghae fault line. Samples at latitudes higher than P-12 are marked with red circles. (b) ^{3}He/^{4}He ratios to distance from the Namsong fault line, which is not prominent. (c) ^{3}He/^{4}He ratios to distance from closer fault lines between the Heunghae and Namsong fault lines. Samples closer to the Namsong fault than the Heunghae fault are marked with blue circles.

Namsong fault system as shown in Figure 5(c). Samples with lower ^{3}He/^{4}He ratios than 1 Ra indicate that the inflow of ^{3}He into the aquifer is less than crustal or atmospheric contributions (Figure 4). Although it is not well known about the exact fault locations in the Yeonil area, previous studies have reported the presence of faults [14 and references therein]. Based on some samples with high ^{3}He/^{4}He ratios (Figure 1), we suggest that there can be a highly permeable fault zone. In this study, we propose to name the Jamyeong fault considering the name of the village called Jamyeong-ri in this area.

4.5. Helium Flux from the Faults. To compare fluid dynamics with other fault systems in the world, helium flow rates and ^{3}He flux were estimated. We calculated helium flow rates from the most reliable mantle helium source from each fault (P-12 for Heunghae fault, PH19-07 for Jamyeong fault, PH19-12 for Namsong fault), following Menzies et al. [46]:

$$qHe = \frac{H_c \rho_c P(He)}{\rho_f [He]_{F.m}} \times \left[\frac{R_s - R_c}{R_m - R_s}\right] \quad (3)$$

where qHe is the helium flow rate (cm/yr); Hc is the crust thickness; ρc and ρf are the density of the crust and the fluid, respectively; $P(He)$ is the current production rate of ^{4}He from crust; $[He]F.m$ is the concentration of helium in the original mantle fluid; Rs, Rc, and Rm represent helium isotopic ratios (^{3}He/^{4}He) of the sample, crust, and mantle, respectively. The crust below the Pohang region was assumed to be a double layer with thicknesses for the upper and middle crust of 12.3 and 15.6 km, respectively [42, 47]. We used the average density values of the middle crust (2.72 g/cm^3) and the upper crust (2.65 g/cm^3) as ρc and the water density (1 g/cm^3) as ρf [48 and references therein]. From Menzies et al. [46], P(He) (ccSTP g^{-1} yr^{-1}) can be obtained as:

$$\mathrm{P(He)} = \rho_c \times \left(1.19 \times 10^{-13} \times [\mathrm{U}] + 2.88 \times 10^{-14} \times [\mathrm{Th}]\right) \times (1 - \Phi)/\Phi \tag{4}$$

where ^{4}He production rates of U and Th are 1.19×10^{-13} ccSTP μg^{-1} yr^{-1} and 2.88×10^{-14} ccSTP μg^{-1} yr^{-1}, respectively; $[U]$ and $[Th]$ are concentrations for U and Th in ppm; Φ is the porosity of the material. By using the average concentration of each layer for U (middle crust: 0.7 ppm and upper crust: 2.7 ppm) and Th (middle crust: 0.63 ppm and upper crust: 10.5 ppm) [48 and references therein], $H_c\rho_c$ P(He) for each crust layer (in equation (3)) was calculated and were added all up. The $[\mathrm{He}]_{\mathrm{F.m}}$ for each sample was calculated using Rs (0.02 Ra), Rm (8 Ra), and helium concentration of each sample.

Each variable is measured or obtained except Φ, resulting in that the helium flow rate is a function of porosity (Φ). The porosity of Yeongnam Massif granodiorite underneath the study area is 0.48% [49]. The porosity measured by wireless logging along PX2 at depth is 5.2% [49], which includes the void volume of fractures. The porosity of the fault zone itself should be higher than that of the fractured basement rock. Therefore, we assumed four different porosity conditions with $\Phi = 0.01, 0.05, 0.1$, and 0.2 which are about 0.2, 1, 2, and 4 times the porosity of the basement rock.

Calculated helium flow rates (qHe) for a given porosity range from 26.95 cm/yr to 128 cm/yr (Heunghae fault), 5.34 cm/yr to 25.37 cm/yr (Namsong fault), and 4.00 cm/yr to 19.02 cm/yr (Jamyeong fault, Table S2). Compared with other global fault zones (1.7 to 12.7 cm/yr of San Andreas Fault; 0.87 cm/yr of North Anatolian Fault; 55 cm/yr of Alpine Fault, New Zealand) [46, 50], faults in the Pohang region show relatively high helium flow rates. To assume that faults in the Pohang region have helium flows of the approximately same magnitude, the porosity of the faults need to be higher than other fault systems. Thus, in the fault zones of the Pohang region, it is believed that the porosity is high, or the helium flow rate is high. With the calculated helium flow rates and measured helium concentration of each sample, we were able to calculate the ^{3}He flux for each sample site by using measured ^{3}He/^{4}He ratios. The ^{3}He flux per unit area (Φ^3He) can be calculated as:

$$\Phi^3\mathrm{He} = \mathrm{qHe} \times \rho\mathrm{f} \times \left[^4\mathrm{He}\right] \times \mathrm{R} \tag{5}$$

where [^{4}He] is measured ^{4}He concentration of each sample; R is helium isotopic composition (^{3}He/^{4}He). The calculated ^{3}He flux values are 120 to 3,000 atoms cm^{-2} sec^{-1} (Heunghae fault), 52 to 1,300 atoms cm^{-2} sec^{-1} (Namsong fault), and 83 to 2,100 atoms cm^{-2} sec^{-1} (Jamyeong fault, Table S2).

In Figure 6, samples related to the Heunghae fault show the correlation between ^{3}He flux and fault. Considering the size of the study area (<10 km from the fault), this trend can be compared with the results near the Futagawa fault (<40 km from the fault) in the Kumamoto area, Kyushu, Japan, where an earthquake of magnitude 7.3 occurred on April 16, 2016 (Sano et al. [6], Table S3, Figure 7). The Heunghae fault zone shows the sharper pattern than the Futagawa fault zone because samples from this area are collected in a smaller area. The maximum flux of the Futagawa fault is 5,600 atoms cm^{-2} sec^{-1}, which is higher than that of the Heunghae area because the sample is close to the fault as well as Mt Aso to supply helium from the nearby magma [6].

Like the helium flow rate, this ^{3}He flux is relatively high compared to other major fault systems, such as 1.7 to 34 atoms cm^{-2} sec^{-1} of the San Andreas Fault, 75 atoms cm^{-2} sec^{-1} of the North Anatolian Fault, and 170 atoms cm^{-2} sec^{-1} of the Alpine Fault, New Zealand [46, 50], showing high porosity in the fault zone or high ^{3}He flux per unit area (Figure 7). Also, this ^{3}He flux is several orders of magnitude higher than the continental ^{3}He flux in steady-state (3.9 to 7.2 atoms cm^{-2} sec^{-1}, from Sano et al. [51]). Therefore, the helium flux results suggest that the Pohang region may have faults comparable to other active fault zones around the world (Figures 1, 6).

5. Conclusions

We first analyzed dissolved gases in groundwater in the Pohang region, South Korea, where the Mw 5.5 earthquake occurred on November 15, 2017. The N_2-Ar-He relationship shows that there is the contribution of the mantle component in the Heunghae and Yeonil area samples, which is similar to that previously reported in fault zones of the southeastern Korean peninsula [9]. However, the dissolved gases in the Sinkwang area are mostly close to atmospheric components. N_2 (32. 5 to 94.0 vol.%) and CO_2 (0.1 to 45.4 vol.%) are present in all areas of the Pohang region, and CH_4 (18.7 to 42.9 vol.%) is observed as a major component in some samples of the Heunghae and Yeonil areas. The results of the stable isotope analysis indicate that N_2 (δ^{15}N = 0.2 to 3.6‰), CO_2 (δ^{13}C = −27.3 to − 16.0‰), and CH_4 (δ^{13}C = −76.1 to − 70.0‰) in the Pohang region are derived from organic material sources at shallow depths. Helium isotope ratios (^{3}He/^{4}He) with mantle signatures (up to 3.83 Ra) are observed in the Heunghae and Yeonil areas except in the Sinkwang area, where atmospheric ^{3}He/^{4}He ratios are mainly observed. Helium originates from the mantle, but the Pohang region, a sedimentary basin formed during the Miocene period, is believed to contain a large amount of organic matter that can be the source for N_2, CO_2, and

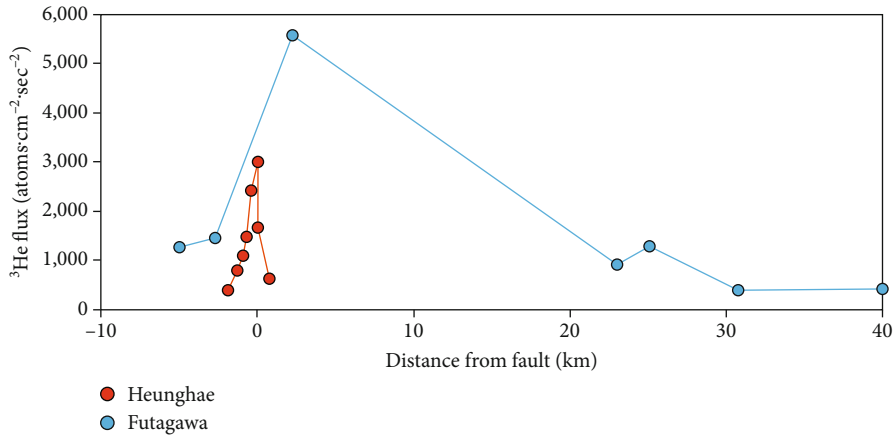

Figure 6: ^{3}He flux values displayed according to the distance from the Heunghae fault in the Pohang region (this study) and the Futagawa fault in the Kumamoto region, Japan [6]. The assumptions about the calculations are described in section 4.5.

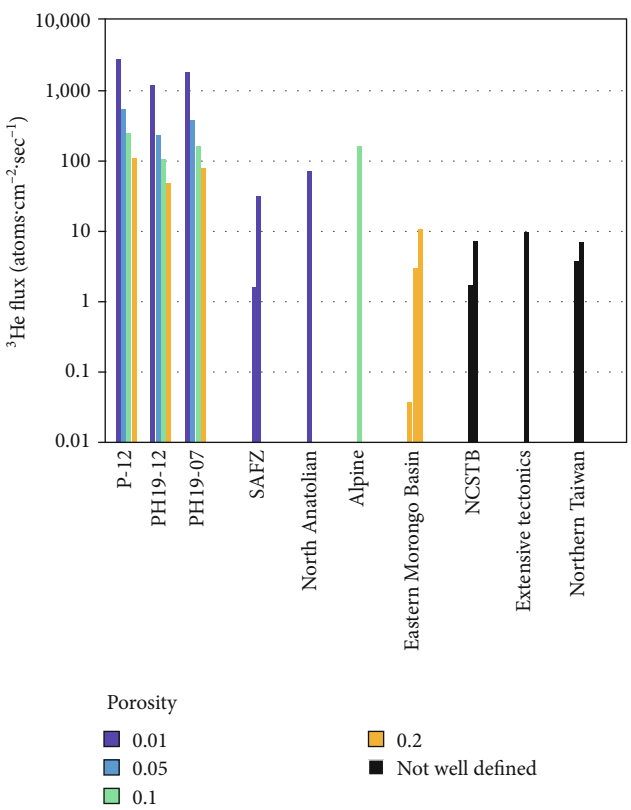

Figure 7: ^{3}He flux of the Heunghae (P-12), Namsong (PH19-12), and Jamyeong faults (PH19-07). Reference data from San Andreas Fault Zone (SAFZ, [50]), North Anatolian Fault[50], Alpine Fault [46], Eastern Morogongo basin [56], North-Central Sicilly thermal basin (NCStb) [57], extensive tectonics settings [22], and Northern Taiwan [51].

CH_4. The distribution of the helium isotope ratio seems to be related to the locations of faults which are permeable passage. Based on the observation, we suggest that the Heunghae, Namsong, and Jamyeong faults in the Pohang region are active faults that release the mantle fluids. Although the Heunghae and Namsong faults are close to the EGS facilities, considering the depths (<10 km) of the 2017 earthquake and aftershocks in the area, the Moho depth (~28 km) is far below, which is similar to the Gyeongju and Ulsan areas [9]. Thus, we propose that there were already active faults extending into the ductile shear zone to release the mantle helium. In order to show that the faults in this area are active, we computed ^{3}He flux (Φ^3He) for the Heunghae (120 to 3,000 atoms cm^{-2} sec^{-1}), Namsong (52 to 1,300 atoms cm^{-2} sec^{-1}), and Jamyeong (83 to 2,100 atoms cm^{-2} sec^{-1}) faults. These values are comparable to those in the regions known as active faults around the world, which may be due to either high porosity or high helium flow rates. Therefore, our results demonstrate that there are active faults in Pohang, especially around the EGS facilities, and will provide important information for future research.

Data Availability

All the data in this study is contained in the tables of both the main manuscript and the Supplementary Materials.

Conflicts of Interest

The authors declare that there is no conflict of interest regarding the publication of this paper.

Acknowledgments

This study was financially supported by the fundamental research project of Korea Institute of Geoscience and Mineral resources (KIGAM) and the National Research Foundation of Korea (NRF) grant funded by the Korea government (MSIT) (NRF-2019R1G1A1002297). We are grateful to Myungok Jung and Kwangtae Kim for their support on the sampling.

Supplementary Materials

Figure S1: (a) relative concentration of CO_2 and pH plot. (b) CO_2/N_2 and pH plot. (c) CO_2/CH_4 and pH plot. (d)

CO_2/CH_4 and concentration of ^4He plot. (e) $CO_2/^3He$ and concentration of ^4He plot. (f) $CO_2/^3He$ and $^3He/^4He$ ratio plot. Figure S2: (a) $CO_2/^3He$ and $\delta^{13}C$ plot. Dashed arrow indicates $CO_2/^3He$ and $\delta^{13}C$ decrease trend due to CO_2 trap, which described in Section 4.2. (b) $\delta^{13}C$ of CO_2 and $\delta^{13}C$ of CH_4 plot (modified from Wfhiticar [34]). Figure S3: helium samples from the Heunghae area (diamond symbol) and the helium isotope and latitude plot. Each symbol is colored by its helium isotope ratio ($^3He/^4He$). The locations of Heunghae (HF) and Namsong (NF) fault lines (dashed line) are described in Section 4.4. The gray triangle indicates the location of the EGS site, and the brown star indicates the location of the Mw 5.5 earthquake. Table S1: $\delta^{15}N$, $N_2/^3He$, and the contribution of three nitrogen endmembers on the Pohang samples: the mantle, sediment, and the air. The $\delta^{15}N$ and $N_2/^3He$ of each endmember and the mixing model are described in Section 4.2. Table S2: the corrected Helium isotope ratio, the concentration of helium in original mantle fluid, the helium flow rate, and the ^3He flux of each fault system. Table S3: the ^4He concentration, corrected $^3He/^4He$ ratio, and ^3He flux of each sample and their distance from related faults, respectively. The data of the Futagawa fault is from Sano et al. [6]. *(Supplementary Materials)*

References

[1] E. L. Majer, R. Baria, M. Stark et al., "Induced seismicity associated with Enhanced Geothermal Systems," *Geothermics*, vol. 36, no. 3, pp. 185–222, 2007.

[2] K. M. Keranen, H. M. Savage, G. A. Abers, and E. S. Cochran, "Potentially induced earthquakes in Oklahoma, USA: links between wastewater injection and the 2011 Mw 5.7 earthquake sequence," *Geology*, vol. 41, no. 6, pp. 699–702, 2013.

[3] A. McGarr, D. Simpson, and L. Seeber, *Case Histories of Induced and Triggered Seismicity, in: International Handbook of Earthquake and Engineering Seismology*, Academic Press LTD, 2002.

[4] Z. E. Ross, B. Idini, Z. Jia et al., "Hierarchical interlocked orthogonal faulting in the 2019 Ridgecrest earthquake sequence," *Science*, vol. 366, no. 6463, pp. 346–351, 2019.

[5] B. M. Kennedy, "Mantle fluids in the San Andreas fault system, California," *Science*, vol. 278, no. 5341, pp. 1278–1281, 1997.

[6] Y. Sano, N. Takahata, T. Kagoshima, T. Shibata, T. Onoue, and D. Zhao, "Groundwater helium anomaly reflects strain change during the 2016 Kumamoto earthquake in Southwest Japan," *Scientific Reports*, vol. 6, no. 1, 2016.

[7] K. Umeda and A. Ninomiya, "Helium isotopes as a tool for detecting concealed active faults," *Geochemistry, Geophysics, Geosystems*, vol. 10, no. 8, 2009.

[8] S. L. Klemperer, B. M. Kennedy, S. R. Sastry, Y. Makovsky, T. Harinarayana, and M. L. Leech, "Mantle fluids in the Karakoram fault: helium isotope evidence," *Earth and Planetary Science Letters*, vol. 366, pp. 59–70, 2013.

[9] H. Lee, H. Kim, T. Kagoshima, J.-O. Park, N. Takahata, and Y. Sano, "Mantle degassing along strike-slip faults in the Southeastern Korean Peninsula," *Scientific Reports*, vol. 9, no. 1, article 15334, 2019.

[10] S. K. Chough, S.-T. Kwon, J.-H. Ree, and D. K. Choi, "Tectonic and sedimentary evolution of the Korean peninsula: a review and new view," *Earth-Science Reviews*, vol. 52, no. 1-3, pp. 175–235, 2000.

[11] J.-M. Kim, "Early Neogene biochemostratigraphy of Pohang Basin: a paleoceanographic response to the early opening of the Sea of Japan (East Sea)," *Marine Micropaleontology*, vol. 36, no. 4, pp. 269–290, 1999.

[12] S. Yi and H. Yun, "Miocene calcareous nannoplankton from the Pohang Basin, Korea," *Palaeontographica Abteilung B*, vol. 237, pp. 113–158, 1995.

[13] T. J. Lee, Y. Song, D.-W. Park, J. Jeon, and W. S. Yoon, "Three dimensional geological model of Pohang EGS pilot site, Korea," *Proceedings of the World Geothermal Congress*, vol. 19, pp. 19–25, 2015.

[14] C. W. Song, *Study on the Evolution of the Miocene Pohang Basin Based on its Structural Characteristics*, Pusan National University, Busan, Korea, 2015, (In Korean with English abstract).

[15] S. S. Chun and S. K. Chough, "Tectonic history of Crataceous sedimentary basins in the southwestern Korean Peninsula and Yellow Sea," *The Sedimentary Basins in the Korean Peninsula and Adjacent Seas*, pp. 60–76, 1992.

[16] D. W. Lee, "Strike–slip fault tectonics and basin formation during the Cretaceous in the Korean Peninsula," *Island Arc*, vol. 8, no. 2, pp. 218–231, 1999.

[17] K. K. Lee, "Summary report of the Korean government commission on relations between the 2017 Pohang earthquake and EGS project," *The Geological Society of Korea*, 2019.

[18] J. Matsuda, T. Matsumoto, H. Sumino et al., "The $^3He/^4He$ ratio of the new internal He Standard of Japan (HESJ)," *Geochemical Journal*, vol. 36, no. 2, pp. 191–195, 2002.

[19] H. Craig, W. B. Clarke, and M. A. Beg, "Excess ^3He in deep water on the East Pacific Rise," *Earth and Planetary Science Letters*, vol. 26, no. 2, pp. 125–132, 1975.

[20] Y. Sano, N. Takahata, and T. Seno, "Geographical distribution of $^3He/^4He$ ratios in the Chugoku District, Southwestern Japan," *Pure and Applied Geophysics*, vol. 163, no. 4, pp. 745–757, 2006.

[21] Y. Sano and H. Wakita, "Geographical distribution of $^3He/^4He$ ratios in Japan: implications for arc tectonics and incipient magmatism," *Journal of Geophysical Research: Solid Earth*, vol. 90, no. B10, pp. 8729–8741, 1985.

[22] M. Ozima and F. A. Podosek, *Noble Gas Geochemistry*, Cambridge University Press, 2002.

[23] H. Lee, T. P. Fischer, J. D. Muirhead et al., "Incipient rifting accompanied by the release of subcontinental lithospheric mantle volatiles in the Magadi and Natron basin, East Africa," *Journal of Volcanology and Geothermal Research*, vol. 346, pp. 118–133, 2017.

[24] J. Zhang, P. D. Quay, and D. O. Wilbur, "Carbon isotope fractionation during gas-water exchange and dissolution of CO_2," *Geochimica et Cosmochimica Acta*, vol. 59, no. 1, pp. 107–114, 1995.

[25] K. Suda, Y. Ueno, M. Yoshizaki et al., "Origin of methane in serpentinite-hosted hydrothermal systems: the CH_4-H_2-H_2O hydrogen isotope systematics of the Hakuba Happo hot spring," *Earth and Planetary Science Letters*, vol. 386, pp. 112–125, 2014.

[26] Y. Taran, D. Morán-Zenteno, S. Inguaggiato, N. Varley, and L. Luna-González, "Geochemistry of thermal springs and geodynamics of the convergent Mexican Pacific margin," *Chemical Geology*, vol. 339, pp. 251–262, 2013.

[27] Y. Sano, N. Takahata, Y. Nishio, T. P. Fischer, and S. N. Williams, "Volcanic flux of nitrogen from the Earth," *Chemical Geology*, vol. 171, no. 3-4, pp. 263–271, 2001.

[28] B. Marty, "Nitrogen content of the mantle inferred from N_2–Ar correlation in oceanic basalts," *Nature*, vol. 377, no. 6547, pp. 326–329, 1995.

[29] B. Marty and L. Zimmermann, "Volatiles (He, C, N, Ar) in mid-ocean ridge basalts: assesment of shallow- level fractionation and characterization of source composition," *Geochimica et Cosmochimica Acta*, vol. 63, no. 21, pp. 3619–3633, 1999.

[30] Y. Sano and B. Marty, "Origin of carbon in fumarolic gas from island arcs," *Chemical Geology*, vol. 119, no. 1-4, pp. 265–274, 1995.

[31] W. Cheng, "Measurement of rhizosphere respiration and organic matter decomposition using natural ^{13}C," *Plant and Soil*, vol. 183, no. 2, pp. 263–268, 1996.

[32] S. M. V. Gilfillan, C. J. Ballentine, G. Holland et al., "The noble gas geochemistry of natural CO_2 gas reservoirs from the Colorado Plateau and Rocky Mountain provinces, USA," *Geochimica et Cosmochimica Acta*, vol. 72, no. 4, pp. 1174–1198, 2008.

[33] M. Schoell, "The hydrogen and carbon isotopic composition of methane from natural gases of various origins," *Geochimica et Cosmochimica Acta*, vol. 44, no. 5, pp. 649–661, 1980.

[34] M. J. Whiticar, "Carbon and hydrogen isotope systematics of bacterial formation and oxidation of methane," *Chemical Geology*, vol. 161, no. 1-3, pp. 291–314, 1999.

[35] L. Hoke, S. Lamb, D. R. Hilton, and R. J. Poreda, "Southern limit of mantle-derived geothermal helium emissions in Tibet: implications for lithospheric structure," *Earth and Planetary Science Letters*, vol. 180, no. 3-4, pp. 297–308, 2000.

[36] T. Torgersen, "Continental degassing flux of ^4He and its variability," *Geochemistry, Geophysics, Geosystems*, vol. 11, no. 6, 2010.

[37] B. M. Kennedy and M. C. van Soest, "Flow of mantle fluids through the ductile lower crust: helium isotope trends," *Science*, vol. 318, no. 5855, pp. 1433–1436, 2007.

[38] Y. Sano, Y. Nakamura, H. Wakita, A. Urabe, and T. Tominaga, "Helium-3 emission related to volcanic activity," *Science*, vol. 224, no. 4645, pp. 150-151, 1984.

[39] C. Chen, D. Zhao, Y. Tian et al., "Mantle transition zone, stagnant slab and intraplate volcanism in Northeast Asia," *Geophysical Journal International*, vol. 209, no. 1, pp. 68–85, 2017.

[40] K. B. Kim and G. D. Lee, "A study on volcanic stratigraphy and fault of Ulleung-do, Korea," *The Journal of Engineering Geology*, vol. 18, no. 3, pp. 321–330, 2008, (In Korean with English abstract).

[41] R. Westaway and N. M. Burnside, "Fault "corrosion" by fluid injection: a potential cause of the November 2017 M_W 5.5 Korean earthquake," *Geofluids*, vol. 2019, Article ID 1280721, 23 pages, 2019.

[42] T. W. Chung, M. Z. Iqbal, Y. Lee, K. Yoshimoto, and J. Jeong, "Depth-dependent seismicity and crustal heterogeneity in South Korea," *Tectonophysics*, vol. 749, pp. 12–20, 2018.

[43] T.-K. Hong, S. Park, and S. E. Houng, "Seismotectonic properties and zonation of the far-eastern Eurasian plate around the Korean Peninsula," *Pure and Applied Geophysics*, vol. 173, no. 4, pp. 1175–1195, 2016.

[44] K. Umeda, Y. Sakagawa, A. Ninomiya, and K. Asamori, "Relationship between helium isotopes and heat flux from hot springs in a non-volcanic region, Kii Peninsula, southwest Japan," *Geophysical Research Letters*, vol. 34, no. 5, pp. 1–5, 2007.

[45] T. Doğan, H. Sumino, K. Nagao, K. Notsu, M. K. Tuncer, and C. Çelik, "Adjacent releases of mantle helium and soil CO_2 from active faults: Observations from the Marmara region of the North Anatolian Fault zone, Turkey," *Geochemistry, Geophysics, Geosystems*, vol. 10, no. 11, 2009.

[46] C. D. Menzies, D. A. H. Teagle, S. Niedermann et al., "The fluid budget of a continental plate boundary fault: quantification from the Alpine Fault, New Zealand," *Earth and Planetary Science Letters*, vol. 445, pp. 125–135, 2016.

[47] K. Y. Kim, J. M. Lee, W. Moon, C. E. Baag, H. Jung, and M. H. Hong, "Crustal structure of the southern Korean peninsula from seismic waves generated by large explosions in 2002 and 2004," *Pure and Applied Geophysics*, vol. 164, no. 1, pp. 97–113, 2007.

[48] B. R. Hacker, P. B. Kelemen, and M. D. Behn, "Continental lower crust," *Annual Review of Earth and Planetary Sciences*, vol. 43, no. 1, pp. 167–205, 2015.

[49] S. Kwon, L. Xie, S. Park et al., "Characterization of 4.2-km-deep fractured granodiorite cores from Pohang Geothermal Reservoir, Korea," *Rock Mechanics and Rock Engineering*, vol. 52, no. 3, pp. 771–782, 2019.

[50] J. T. Kulongoski, D. R. Hilton, P. H. Barry, B. K. Esser, D. Hillegonds, and K. Belitz, "Volatile fluxes through the Big Bend section of the San Andreas Fault, California: helium and carbon-dioxide systematics," *Chemical Geology*, vol. 339, pp. 92–102, 2013.

[51] Y. Sano, H. Wakita, and C. W. Huang, "Helium flux in a continental land area estimated from $^3He/^4He$ ratio in northern Taiwan," *Nature*, vol. 323, no. 6083, pp. 55–57, 1986.

[52] W. B. F. Ryan, S. M. Carbotte, J. O. Coplan et al., "Global multi-resolution topography synthesis," *Geochemistry, Geophysics, Geosystems*, vol. 10, no. 3, 2009.

[53] H. Lee, J. D. Muirhead, T. P. Fischer et al., "Massive and prolonged deep carbon emissions associated with continental rifting," *Nature Geoscience*, vol. 9, no. 2, pp. 145–149, 2016.

[54] J. L. Lewicki and S. L. Brantley, "CO_2 degassing along the San Andreas Fault, Parkfield, California," *Geophysical Research Letters*, vol. 27, no. 1, pp. 5–8, 2000.

[55] Y. Sano, N. Kinoshita, T. Kagoshima et al., "Origin of methane-rich natural gas at the West Pacific convergent plate boundary," *Scientific Reports*, vol. 7, no. 1, article 15646, 2017.

[56] J. T. Kulongoski, D. R. Hilton, and J. A. Izbicki, "Source and movement of helium in the eastern Morongo groundwater Basin: the influence of regional tectonics on crustal and mantle helium fluxes," *Geochimica et Cosmochimica Acta*, vol. 69, no. 15, pp. 3857–3872, 2005.

[57] A. Caracausi and A. Sulli, "Outgassing of mantle volatiles in compressional tectonic regime away from volcanism: the role of continental delamination," *Geochemistry, Geophysics, Geosystems*, vol. 20, no. 4, pp. 2007–2020, 2019.